IEEE Access
Multidisciplinary | Rapid Review | Open Access Journal

Received December 24, 2021, accepted January 6, 2022, date of publication January 11, 2022, date of current version January 20, 2022.

Digital Object Identifier 10.1109/ACCESS.2022.3141915

A Robust Design Method for Optimal Engine Operating Zone Design of Plug-in Hybrid Electric Bus

YUJIE LIU[1], QUN SUN[1], QIANG HAN[1], HAIGANG XU[2], WENXIAO HAN[1], AND HONG-QIANG GUO[1]

[1]School of Mechanical and Automotive Engineering, Liaocheng University, Liaocheng 252059, China
[2]Shandong Shifeng (Group) Company Ltd., Liaocheng, Shandong 252899, China

Corresponding author: Qun Sun (sunqun@lcu.edu.cn)

This work was supported by the Natural Science Foundation of Shandong Province under Grants ZR2020ME128 and ZR2021MF125.

ABSTRACT The optimal engine operating zone of energy management plays an important role in the fuel economy improvement of Plug-in hybrid electric buses. However, the existing investigations usually design the engine operating zone by experience. This paper proposes a robust design method for the robust and optimal design of the engine operating zone. Firstly, a nonlinear model predictive control (NMPC)-based energy management together with a single-point preview SOC (state of charge) plan method is designed. Then, a Taguchi robust design model is designed to find the optimal engine operating zone by taking the energy management as underlying solving module. Particularly, the noises of driving cycles and stochastic vehicle mass are considered to improve the robust performance of the engine operating zone. Finally, The Monte Carlo Simulation is deployed to verify the robustness and optimal performances of the designed engine operating zone. Simulation results demonstrate that the proposed method is beneficial to the fuel economy improvement, where the fuel economy can be averagely improved by 9.10% compared with the experienced designed engine operating zone, and can be averagely improved by 16.34% compared with the rule-based energy management strategy.

INDEX TERMS Energy management, engine operating zone, nonlinear model predictive control, plug-in hybrid electric bus, Taguchi robust design.

I. INTRODUCTION

With the increasing energy crisis and environmental pollution problems, many countries have launched relevant policies to promote the development of new energy vehicle [1], [2]. Plug-in hybrid electric vehicle (PHEV) develops rapidly because it can incorporate the merits of the pure electric vehicle (PEV) and the hybrid electric vehicle (HEV) [3], [4]. Moreover, energy management strategy(EMS) is the key of the fuel economy improvement to the PHEV [5], [6].

EMS can be divided into rule-based, optimization-based, adaptive control and reinforcement learning-based (RL) strategies [7], [8]. In terms of the rule-based strategy, Li *et al.* proposed a torque-leveling threshold-changing strategy, which can ensure the engine operates at an efficient operating point [9]. Xu *et al.* proposed a double fuzzy control strategy for a parallel hybrid electric vehicle, where the genetic algorithm (GA) is deployed to optimize the fuzzy control rules. The simulation results demonstrated that the optimized fuzzy control rules can adjust the operating points of the engine, and improve the fuel economy of the vehicle [10]. Zhou et.al proposed a parameter selection method to optimize rule-based energy management based on dynamic programming. The results showed that the optimized method can improve the operating points distribution of the engine, and improve the fuel economy of the vehicle [11]. In terms of the optimization-based strategy, Hu *et al.* presented a dynamic programming (DP) algorithm to distribute the power between engines and batteries for a heavy-duty hybrid electric vehicle. The simulation results demonstrated that the fuel economy can be greatly improved due to the better distribution of the operation points of engine [12].

The associate editor coordinating the review of this manuscript and approving it for publication was Chandan Kumar.

Solouk *et al.* presented a Pontryagin's Minimum Principle (PMP)-based energy management, where the fuel economy of the vehicle can be greatly improved, because the engine operating points can be located in an efficient zone [13]. Liu *et al.* proposed an improved equivalent fuel consumption minimization strategy (ECMS) for a hybrid electric vehicle, where the fuel economy can be improved by adjusting the engine operating point to a high-efficiency zone during the acceleration process [14]. In terms of the adaptive control strategy, Wang *et al.* presented a stochastic model predictive control (SMPC)-based energy management, to improve the operating points distribution of an engine [15]. Liu *et al.* proposed an adaptive hierarchical energy management for a PHEV, which can prevent the engine from operating in the inefficient zone while reducing the fuel consumption of the vehicle [16]. In terms of the RL-based strategy, Zhang *et al.* presented a Q-function-based energy management, where the results indicated that the operating points of the engine can be concentrated in the high-efficiency zone [17]. According to the above research results, the distribution of the engine operating points plays an important role in the improvement of the fuel economy.

Therefore, if the engine operating zone can be optimally designed in advance, the fuel economy may be greatly improved. Fortunately, many investigations have paid attention to this problem [18]. Bagwe *et al.* proposed a method for the optimization of the engine operating zone based on adaptive rule-based energy management. The results showed that it can prevent the engine from operating in highly inefficient zones and reduce the total equivalent fuel consumption of the vehicle [19]. Zhang *et al.* proposed an engine operating zone design method based on a designed optimal operating curve, where the fuel economy can be greatly improved. Moreover, the problem of starting and stopping the engine frequently can be reduced [20]. Guo *et al.* and Shabbir *et al.* proposed a method to locate the engine points in the high-efficiency zone, by which the fuel economy and the driving performance can be greatly improved [21], [22].

However, the above methods ignored the noises of driving cycles and stochastic vehicle mass. In fact, the above noises have a great effect on the design of the engine operating zone [23]. For example, different driving cycles imply different power requirements of the vehicle. Different power requirements imply that the optimal engine operating zone should also be different. Otherwise, the fuel economy of the vehicle may be deteriorated. Similarly, different bus routes imply different distributions of the vehicle mass due to the stochastic distribution characteristic of the passengers in different bus stops, and different distributions of the vehicle mass imply different distributions of the power requirement [24].

This paper exclusively proposes a robust design method for the robust and optimal design of the engine operating zone of a Plug-in hybrid electric bus (PHEB), by considering the noises of the driving cycles and stochastic vehicle mass. The main contributions are summarized as follows:

1) A NMPC-based energy management strategy together with a single-point preview SOC (state of charge of battery) plan method is proposed, to realize the adaptive energy management control.

2) A Taguchi robust design (TRD) method is proposed for the robust and optimal design of the engine operating zone in consideration of the noises of driving cycles and stochastic vehicle mass. Meanwhile, a reliable verification method is deployed to verify the performance of the designed energy management, based on the Monte Carlo Simulation (MCS).

The paper is organized as follows. The description of PHEB is given in Section II. The NMPC-based energy management is detailed in Section III. The TRD and MCS methods for the engine operating zone are introduced in section IV. The results and discussions are given in Section V, and the conclusions are drawn in Section VI.

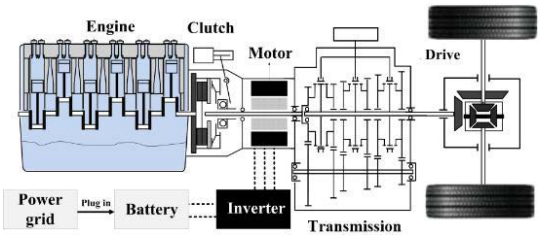

FIGURE 1. The diagram of the PHEB with signal-parallel hybrid powertrain.

TABLE 1. The detailed parameters of the PHEB.

Item	Description
Vehicle	Length (m): 11; Curb mass (kg):11500
Passengers	Maximum number: 55; Passenger mass (kg): 70
AMT	Speed ratios: 6.39, 3.97, 2.4, 1.48, 1, 0.73
Final drive	Speed ratio: 5.571
Engine	Max torque (Nm): 761
	Max power (kW): 148.4
Motor	Max torque (Nm): 850
	Max power (kW): 130.9
Battery	Capacity (Ah): 40

II. MODEL DESCRIPTIONS FOR PHEB

A. CONFIGURATIONS AND MODELS OF THE PHEB

As shown in Fig. 1, the PHEB is signal-paralleled, where an engine, a clutch, an electric motor (EM), and an automatic manual transmission (AMT) are sequentially assembled in the driveline. It can realize five typical working modes, including EM driving mode, engine driving mode, hybrid driving mode, engine charging mode, and regenerative braking mode. The detailed parameters of the PHEB are shown in Table 1.

B. VEHICLE DYNAMIC

The energy consumption of the PHEB is mainly impacted by longitudinal model [25]. Based on the longitudinal dynamics

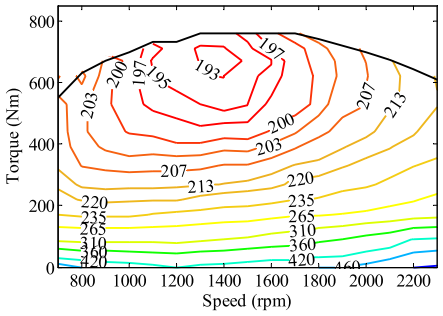

FIGURE 2. The fuel consumption rate MAP of the engine.

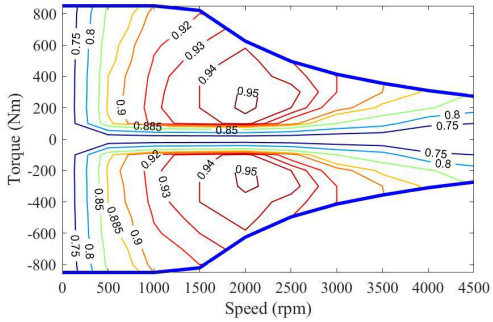

FIGURE 3. The efficiency MAP of the EM.

equation, the relationship between the torque of wheel and the output torque of two power sources is written as:

$$\begin{aligned} T_{\mathrm{w}} &= \eta_{\mathrm{t}} \cdot i_{\mathrm{AMT}} \cdot i_0 \left(T_{\mathrm{e}} + T_{\mathrm{m}}\right) + T_{\mathrm{b}} \\ &= (m_{\mathrm{v}} + m_{\mathrm{p}}) g r f_{\mathrm{r}} \cos\theta + \frac{C_{\mathrm{D}} A r v^2}{21.15} \\ &\quad + (m_{\mathrm{v}} + m_{\mathrm{p}}) g r \sin\theta + \delta (m_{\mathrm{v}} + m_{\mathrm{p}}) \frac{d\tilde{v}}{dt} r \end{aligned} \tag{1}$$

where T_{w} denotes the torque of wheel; η_{t} denotes transmission efficiency; i_{AMT} and i_0 denote gear ratio of the AMT and the final drive ratio, respectively; T_{e} and T_{m} denote the engine torque and the EM torque, respectively; T_{b} is the braking torque acting on the wheel; g, θ and f_{r} denote the gravity acceleration, angle of the road slope and rolling resistance coefficient, respectively. The slope is not considered in this paper, so θ is 0;, C_D, A and v denote the air resistance coefficient, windward area and velocity of the vehicle, respectively;δ denotes the conversion coefficient of rotating mass; r denotes the radius of the wheel; m_{v} and m_{p} denote the empty vehicle mass and the passenger mass, respectively.

C. ENGINE MODEL

As shown in Fig. 2, the engine is a highly complex system, the engine dynamic model, which reflects the transient characteristics of all parts, is not the research focus of this paper. Therefore, the experimental approach is adopted to model the engine, and the dynamic characteristics the engine are neglected. The instantaneous fuel consumption of engine can be calculated by the fuel consumption rate in (2). The fuel consumption is obtained through looking up the fuel consumption rate MAP of the engine,

$$\dot{m}_{\mathrm{e}} = \frac{T_{\mathrm{e}} \cdot n_{\mathrm{e}}}{9550} \cdot \frac{b_{\mathrm{e}}\left(T_{\mathrm{e}}, n_{\mathrm{e}}\right)}{3600} \tag{2}$$

where $\dot{m}_{\mathrm{e}}$ denotes the instantaneous fuel consumption; n_{e} denotes the speed of the engine; $b_{\mathrm{e}}(T_{\mathrm{e}}, n_{\mathrm{e}})$ denotes the fuel consumption rate. During the driving cycle, the fuel consumption performance can be optimized by limiting the engine operating point to the high efficiency zone.

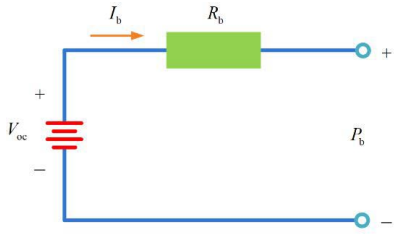

FIGURE 4. The equivalent circuit of simplified battery model.

D. MOTOR MODEL

Similar to engine model, the dynamic performance of the EM is also neglected. Since only one EM is used in the plug-in hybrid electric powertrain, it can be used as an electromotor or a generator during driving or braking modes, respectively. The power consumption of the EM can be calculated by

$$P_{\mathrm{m}} = \begin{cases} \left(n_{\mathrm{m}} \cdot T_{\mathrm{m}}\right) / \left(\eta_{\mathrm{m}} \cdot 9550\right), & E\text{lectromotor} \\ \left(n_{\mathrm{m}} \cdot T_{\mathrm{m}} \cdot \eta_{\mathrm{m}}\right) / \left(9550\right), & G\text{enerator} \end{cases} \tag{3}$$

where P_{m} denotes the power of the EM; n_{m} denotes the speed of the EM; η_{m} denotes the efficiency of the EM, which can be interpolated by the efficiency MAP of the EM, as shown in Fig. 3.

E. BATTERY MODEL

As shown in Fig. 4, the battery model is simplified as an equivalent circuit with a voltage source and a resistance. The dynamics of battery SOC and the internal current can be described as

$$\dot{SOC} = -I_{\mathrm{b}} / Q_{\mathrm{b}} \tag{4}$$

$$I_{\mathrm{b}} = \frac{V_{\mathrm{OC}} - \sqrt{V_{\mathrm{OC}}^2 - 4 P_{\mathrm{b}} \cdot R_{\mathrm{b}}}}{2 R_{\mathrm{b}}} \tag{5}$$

where P_{b} denotes the power of battery; V_{OC} denotes the open-circuit voltage; Q_{b} denotes the battery capacity; R_{b} denotes the internal resistance.

III. THE FORMULATION OF THE NMPC-BASED ENERGY MANAGEMENT

The fuel minimization problem of the PHEB can be taken as a nonlinear and constrained optimal control problem [26]. A NMPC-based energy management is proposed in this paper

because its performance in dynamic control is excellent [27]. The detailed description of the method is listed as follows.

Firstly, in the discrete time domain, the PHEB system can be described as follows:

$$\begin{cases} x(k+1) = A(k)x(k) + Bu(k) + Dw(k) \\ y(k) = Cx(k) \end{cases} \tag{6}$$

where $x(k)$, $u(k)$, $w(k)$ and $y(k)$ denote the discrete time state variables, control variables, disturbance variables and output variables, respectively. They can be expressed as follows:

$$\begin{cases} x(k) = [v(k), T_e(k), T_m(k), T_b(k), SOC(k)]^T \\ u(k) = [T_e^*(k), T_m^*(k)]^T \\ w(k) = [T_{driver}(k), F_f(k)]^T \\ y(k) = [v(k), SOC(k)]^T \end{cases} \tag{7}$$

where $v(k)$ is the vehicle velocity; $T_e(k)$ and $T_m(k)$ denote the torques of engine and EM, respectively; $T_b(k)$ denotes the mechanical braking torque on wheels. $SOC(k)$ is the state of charge of battery; $T_e^*(k)$ and $T_m^*(k)$ is the desired torque of engine and EM, respectively; $T_{driver}(k)$ is the driver demand torque acting on the wheels of the vehicle; $F_f(k)$ is the total resistance of vehicle; k denotes the times of kT_s, where T_s represent the sample time.

In addition the equation can be derived, as shown at the bottom of next page, where τ_e, τ_m and τ_b denote the time-delay coefficient of the engine, motor and mechanical braking system, respectively. Since the characteristics of battery SOC is nonlinear, (6) is a nonlinear model. The derivate of SOC is relevant to the vehicle velocity, the torque of motor, and SOC, so we define the $f_N(k)$ in the coefficient matrix $A(k)$.

Because the electric energy of battery is always cheaper than petroleum, it is usually hoped that the electric energy of battery can be exhausted (to the lowest level SOC^{Min}) in the destination of driving cycle to reduce fuel consumption. Therefore, the cost function is designed as follow:

$$J = \sum_{k=1}^{N} \dot{m}_e(x(k)) \cdot T_s + p(SOC(N)) \tag{8}$$

where N is the length of the predictive horizon; $p(SOC(N))$ penalizes the deviation of SOC at the end of the predictive horizon from a value of SOC reference trajectory, which can guarantee the electric energy can be consumed reasonable.

The vehicle constraint conditions of the cost function are shown below.

$$\begin{cases} SOC^{Min} \le SOC(k) \le SOC^{Max} \\ n_e^{Min} \le n_e(k) \le n_e^{Max} \\ n_m^{Min} \le n_m(k) \le n_m^{Max} \\ T_e^{Min} \le T_e(k) \le T_e^{Max} \\ T_m^{Min} \le T_m(k) \le T_m^{Max} \end{cases} \tag{9}$$

where SOC^{Min} and SOC^{Max} denote the corresponding boundaries of $SOC(k)$, respectively; n_e^{Min}, n_e^{Max} and n_m^{Min}, n_m^{Max} denote the corresponding boundaries of $n_e(k)$ and $n_m(k)$, respectively; T_e^{Min}, T_e^{Max} and T_m^{Min}, T_m^{Max} denote the corresponding boundaries of $T_e(k)$ and $T_m(k)$, respectively.

As shown in Fig. 5, the single-point preview SOC plan method is proposed. In order to make the SOC reach the objective of 0.3 at the destination of the route and avoid the influence of the stochastic characteristic of driving conditions, the SOC reference trajectory will be dynamically planed by linear method at every fixed distance step (the 0.05 normalized travelling distances). Here, the initial point is the SOC value corresponding to the starting position of the fixed distance step, and the terminal point is $(1, 0.3)$. The SOC reference trajectory can be described as:

$$SOC_r(k) = \frac{d_r(k) - 1}{d_f(k-1) - 1}(SOC_f(k-1) - 0.3) + 0.3 \tag{10}$$

where SOC_r and d_r denote the reference SOC and traveled normalized distance at current time step, respectively; SOC_f and d_f denote the feedback of the SOC and the normalized distance from the previous time step, respectively. Here, the SOC_f and d_f will be updated only at the starting position of the fixed distance step.

As shown in Fig. 6, the specific procedures of NMPC-based energy management are listed as follows.

1) Firstly, the driver model is constructed based on PID controller, which is used to obtain pedals opening based on the error between current and reference velocities. According to the above pedals opening, the demand torque can be obtained by looking-up table, and will be delivered to the prediction module as the start point of control horizon.

2) Secondly, according to the assumption that the predicted torque decreases exponentially, the demand torque sequences over the prediction horizon will be predicted in the prediction module. It can be expressed as follows:

$$T_{driver}(k+i) = T_{driver}(k)e^{\left(\frac{(-i*0.1+0.1)*\tau}{\tau_d}\right)} \quad i = 1, 2, \ldots, N \tag{11}$$

where $T_{driver}(k)$ is the known at the current step; $T_{driver}(k+i)$ is the driving demand torque over the prediction horizon; τ is the sample time and τ_d is the decay coefficient; N is the length of the prediction. After solving the demand torque sequences, the velocity forecast sequences are estimated by the vehicle longitudinal dynamic equations.

3) Thirdly, the optimal torque sequences can be solved by DP, by taking the reference SOC, the velocity forecast sequences and the PHEB states as inputs of optimization module. In addition, the PHEB states are composed by SOC, gear position, velocity, resistance force of road, etc. More importantly, the first element of the optimal torque sequences will be extracted to the PHEB model to solve the next states.

4) Then, taking the SOC, traveled normalized distance and feedback normalized distance from the PHEB model as inputs of the SOC reference trajectory planning module, the

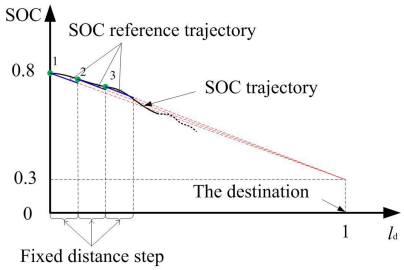

FIGURE 5. The single-point preview SOC plan method.

reference SOC of the next states will be predicted, which will be delivered to the optimization module.

5) Finally, repeat steps (1) to (4).

IV. THE FORMULATION OF THE ROBUST DESIGN METHOD

As shown in Fig. 7, the robust design method is mainly divided into two steps. The first step is to design the engine operating zone based on TRD. Here, the engine operating zone is designed as the control factor; the historical driving cycles and the stochastic vehicle mass (the stochastic passenger mass) are designed as the noise factors. Then the control factors and the noise factors are combined to design the inter-outer table. Finally, based on the NMPC, the signal-to-noise ratio (SNR) can be calculated and the designed engine operating zone can be obtained by analyzing the SNR. The second step is to verify the designed engine operating zone obtained by the TRD based on the MCS. Here, the historical driving cycles and stochastic vehicle mass are designed as random input variables, and the terminal SOC are designed as responses of the NMPC. Based on the responses of the NMPC, once the better robustness of the designed engine operating zone is guaranteed, it will be applied to the PHEB that taking the NMPC-based energy management as

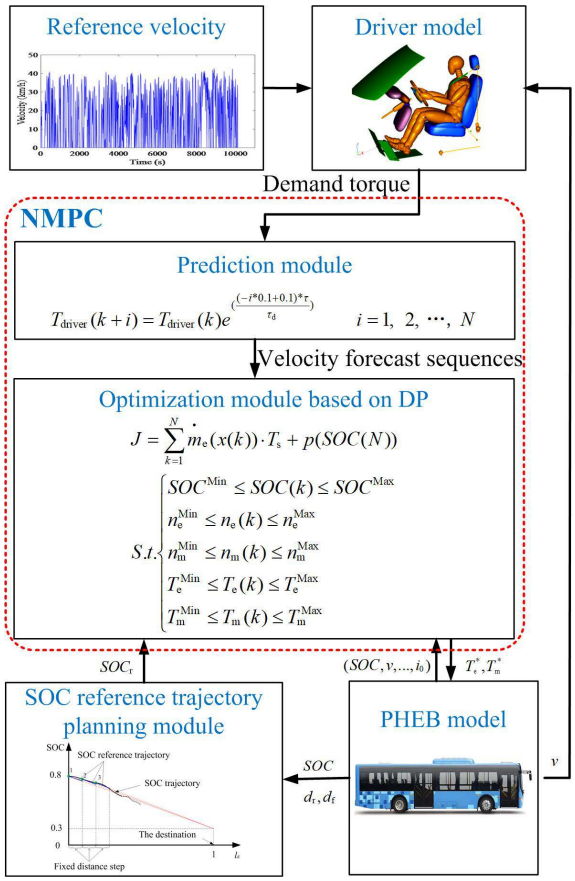

FIGURE 6. The framework of NMPC-based energy management.

$$A(k)=\begin{bmatrix} 1 & \frac{\eta_t i_{AMT} i_0}{\delta(m_v+m_p)r} & \frac{\eta_t i_{AMT} i_0}{\delta(m_v+m_p)r} & \frac{1}{\delta(m_v+m_p)r} & 0 \\ 0 & 1-\frac{1}{\tau_e} & 0 & 0 & 0 \\ 0 & 0 & 1-\frac{1}{\tau_m} & 0 & 0 \\ 0 & 0 & 0 & 1-\frac{1}{\tau_b} & 0 \\ f_N(k) & 0 & f_N(k) & 0 & 1+f_N(k) \end{bmatrix},$$

$$B=\begin{bmatrix} 0 & 0 \\ \frac{1}{\tau_e} & 0 \\ 0 & \frac{1}{\tau_m} \\ -\frac{\eta_t i_{AMT} i_0}{\tau_b} & -\frac{\eta_t i_{AMT} i_0}{\tau_b} \\ 0 & 0 \end{bmatrix},\quad C=\begin{bmatrix} 1 & 0 & 0 & 0 & 0 \\ 0 & 0 & 0 & 0 & 1 \end{bmatrix},\quad D=\begin{bmatrix} 0 & -\frac{1}{\delta(m_v+m_p)} \\ 0 & 0 \\ 0 & 0 \\ \frac{1}{\tau_b} & 0 \\ 0 & 0 \end{bmatrix},$$

$$f_N(k)=-\frac{V_{OC}-\sqrt{V_{OC}^2-4P_b\cdot R_b}}{2Q_b R_b\,(v(k)+T_m(k)+SOC(k))}.$$

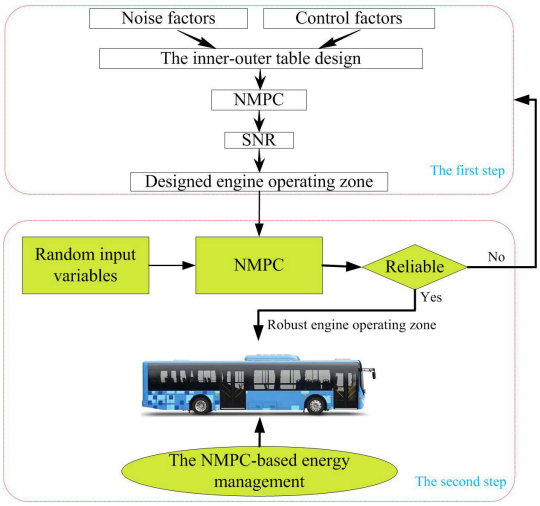

FIGURE 7. The diagram of the robust design method.

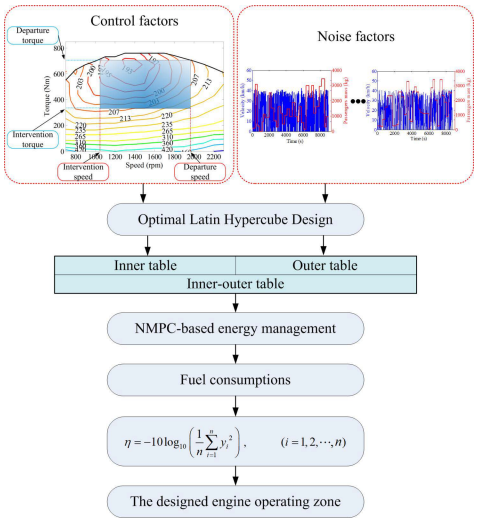

FIGURE 8. The diagram of the Taguchi robust design.

underlying solving module; otherwise, the above steps are repeated.

A. THE FORMULATION OF THE TAGUCHI ROBUST DESIGN

As shown in Fig. 8, the detailed diagram of Taguchi Robust Design is described. Firstly, the control factors are designed based on the Optimal Latin Hypercube Design (Opt-LHD) to structure the inner table of inner-outer table; the noise factors are designed based on the Opt-LHD to structure the outer table of inner-outer table. Here, the control factors are represented in detail as the intervention speed, departure speed, intervention torque and departure torque of engine; the noise factors are represented in detail as the historical driving cycles and the mass of passenger in different road segments. Secondly, the inter-outer table is applied to the NMPC-based energy management to calculate fuel consumptions for each combination of control factors and noise factors.

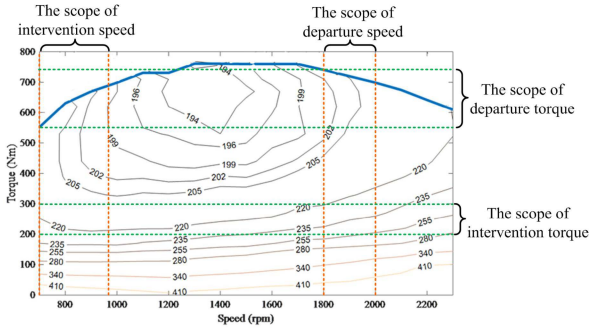

FIGURE 9. The scope of each control factors.

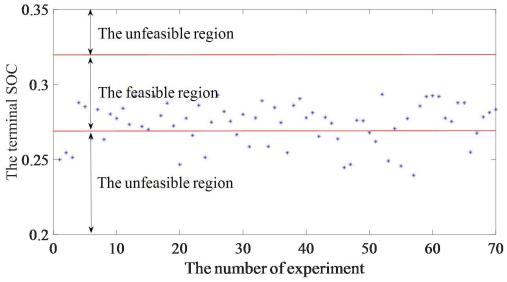

FIGURE 10. The terminal SOCs corresponding to different noise factors.

Then, based on the above calculation results, the SNRs corresponding to each control factors are calculated. At last, the designed engine operating zone is obtained by analyzing the SNRs.

1) TRD CALCULATION METHOD

The SNR is designed as an evaluation index that is used to evaluate the robustness of the system. The higher SNR of the system means less quality loss and higher robustness. In this case, based on analysis of the SNR, the impact of noises on the system response will be reduced by designing control factors. For static system, SNR has three different evaluation indexes, which include the larger-the-better, smaller-the-better (STB) and the nominal-the-best. Because the NMPC-based energy management problem mainly belongs to the static system and its purpose is to minimize the average fuel consumption, the STB is applied for SNR. It can be expressed by the following equation:

$$\eta = -10\log_{10}\left(\frac{1}{n}\sum_{i=1}^{n} y_i^2\right) \quad (i = 1, 2, \ldots, n) \tag{12}$$

where η denotes the SNR of the STB; y_i denotes the fuel consumption at every instant. n denotes the number of experiments. In addition, the quality loss function is defined as follows.

$$L(y) = \beta y^2, \quad y \geq 0 \tag{13}$$

where $L(y)$ denotes the quality loss; β denotes the coefficient of the quality loss; y denotes the quality value.

TABLE 2. The inner-outer table.

The experiment sequences	The design of control factors (The inner table)				The design of noise factors (The outer table)				Calculation results
1	con1_1	con1_2	con1_3	con1_4	cyc1_1 cyc2_1 . . . cyc50_1	m1_1 m2_1 . . . m50_1	m1_2 m2_2 . . . m50_2	… m1_32 … m2_32 … . … . … . … m50_32	η_1 and $L_1(y)$
2	con2_1	con2_2	con2_3	con2_4	cyc1_1 cyc2_1 . . . cyc50_1	m1_1 m2_1 . . . m50_1	m1_2 m2_2 . . . m50_2	… m1_32 … m2_32 … . … . … . … m50_32	η_2 and $L_2(y)$
…	…	…	…	…	…	…	…	… …	…
60	con60_1	con60_2	con60_3	con60_4	cyc1_1 cyc2_1 . . . cyc50_1	m1_1 m2_1 . . . m50_1	m1_2 m2_2 . . . m50_2	… m1_32 … m2_32 … . … . … . … m50_32	η_{60} and $L_{60}(y)$

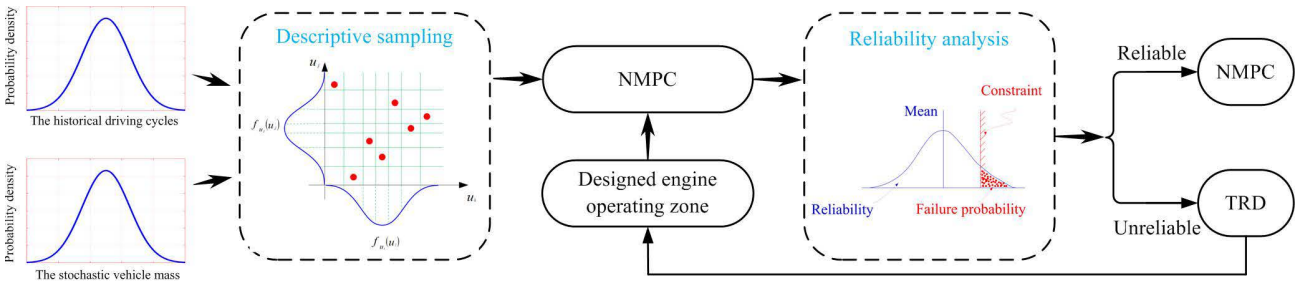

FIGURE 11. The framework of MCS reliable verification.

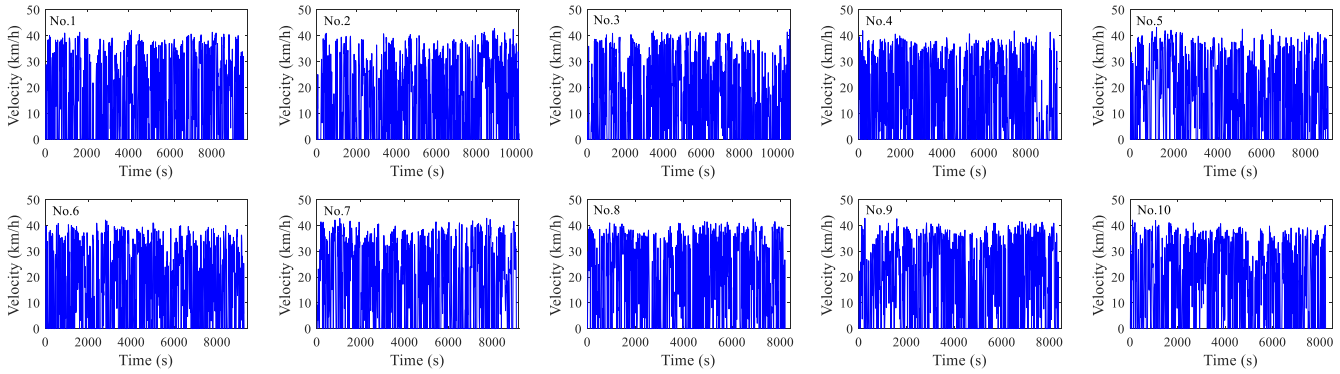

FIGURE 12. The historical driving cycles from No.1 to No.10.

2) THE INNER-OUTER TABLE DESIGN

As shown in Table 2, the inner table is composed of 60 sets of control factors. The scopes of each control factors are shown in Fig. 9. The outer table is composed of 50 sets of noise factors. Moreover, 50 energy management calculations will be executed to each control factor, based on the noise factors. The SNRs and the quality losses for each control factors can be calculated by (12) and (13), respectively.

B. MCS RELIABLE VERIFICATION

As shown in Fig. 10, corresponding to the different noise factors, the terminal SOCs based on the result of TRD may

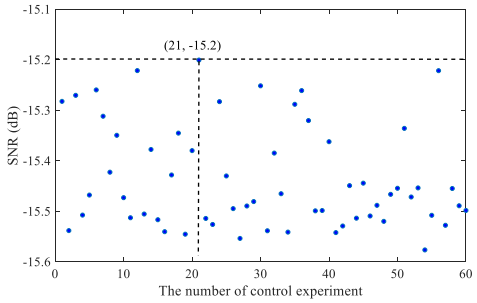

FIGURE 13. The SNRs of experiments.

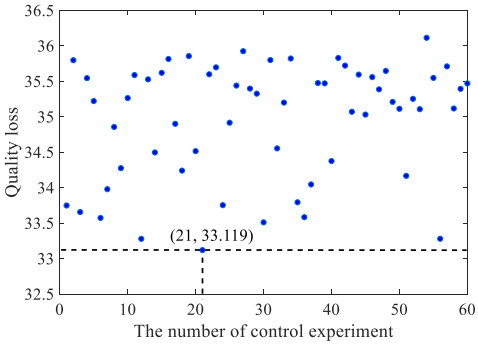

FIGURE 14. The quality losses of experiments.

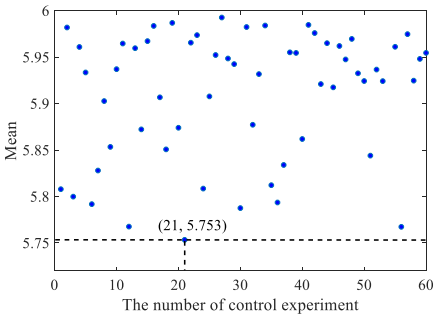

FIGURE 15. The means of fuel consumption.

TABLE 3. The optimal control sequence based on TRD.

Control sequences	Value
Intervention torque (Nm)	220
Departure torque (Nm)	687.69
Intervention speed (rpm)	961
Departure speed (rpm)	1919

deviate from the feasible region. Therefore, the robustness of the result of TRD should be verified. As shown in Fig. 11, the reliable verification based on MCS is described. Firstly, the historical driving cycles and the stochastic vehicle mass are designed as random variables by the probability model of normal, and are sampled by the descriptive sampling method. Secondly, the sampling results and the designed engine operating zone of the TRD are delivered to the NMPC-based energy management to calculate the terminal SOCs for

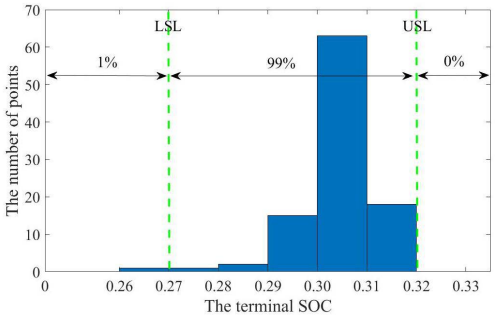

FIGURE 16. The feasible and unfeasible region distribution.

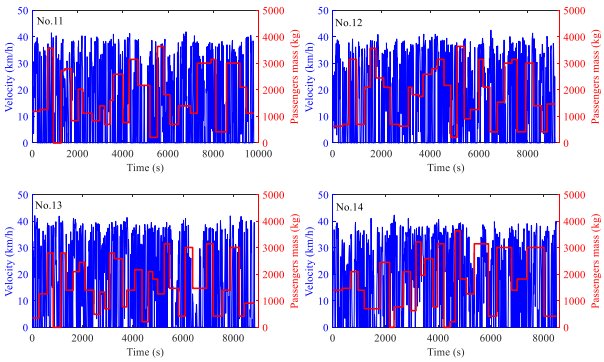

FIGURE 17. The combined driving cycles from No. 11 to No. 14.

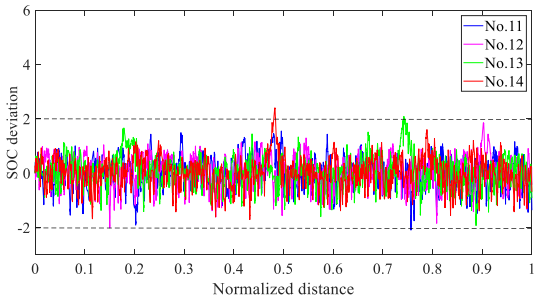

FIGURE 18. The deviations between the actual SOC and the reference SOC.

every combination of random variables. Finally, analyzing the reliability of the designed engine operating zone based on above calculation results, once the robustness is satisfied, the robust engine operating zone can be employed in the NMPC-based energy management; otherwise, it needs to be redesigned by the TRD.

V. RESULTS AND DISCUSSION

A. TRD RESULTS AND DISCUSSION

As shown in Fig. 12, 10 historical driving cycles (from No.1 to No.10) are downloaded from remote monitoring system, and are used to design the robust engine operating zone. The maximum velocities of the 10 driving cycles do not exceed 50 km/h, and the maximum driving distances do not exceed 47 km.

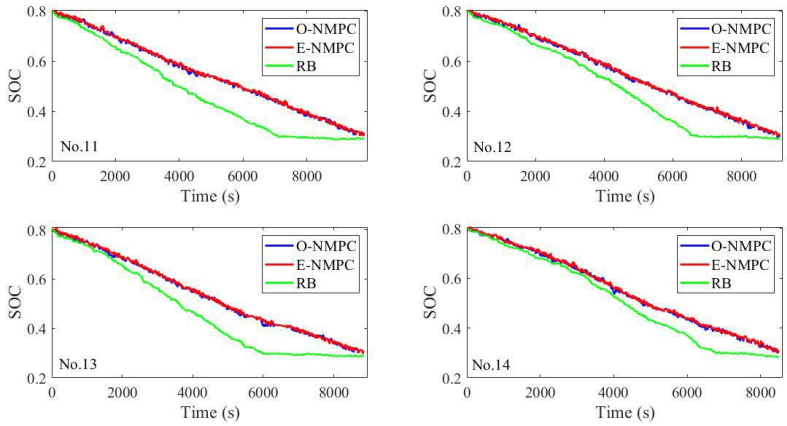

FIGURE 19. The SOC trajectories of the control strategies.

As shown in Fig. 13, the maximum value of SNR in all experiments comes from experiment 21, and its value is −15.2. As shown in Fig. 14, the minimum value of quality loss comes from experiment 21, whose value is 33.119. As mentioned above, the higher SNR implicates less quality loss and higher robustness. Thus, based on the analysis of Fig. 13 and Fig. 14, the experiment 21 possesses the preferable system and higher robustness. Meanwhile, the Fig. 15 shows that the minimum mean of fuel consumption is also from experiment 21, whose value is 5.753. It implies that the experiment 21 has preferable fuel economy compared with other experiments. Eventually, the optimal control sequences based on TRD are shown in Table 3.

B. MCS VERIFICATION RESULTS AND DISCUSSION

The designed engine operating zone based on TRD is verified by MCS. As shown in Fig. 16, the feasible region and the unfeasible region are divided by the lower specification limit (LSL) and the upper specification limit (USL), whose values are 0.27 and 0.32, respectively. Based on the MCS results, the failure probabilities of LSL and USL are 1% and 0%, respectively, and the total reliable probability is 99%, which indicates that the designed engine operating zone has high reliability and good robustness.

C. THE SOC FOLLOWING PERFORMANCE RESULTS AND DISCUSSION

As shown in Fig. 17, 4 combined driving cycles (the combination of driving cycles and the stochastic passenger mass) from No.11 to No.14 are designed to verify the tracking accuracy of the actual SOC to the reference SOC. Here, the stochastic passenger mass in different road segments is obtained based on the Opt-LHD method, and the historical driving cycles are obtained from remote monitoring system. As shown in Fig. 18, most of the deviations between the actual SOC (Percentile System) and the reference SOC (Percentile System) locate in the scope of [−2, 2]. This implies that the designed SOC reference trajectory is reasonable for the NMPC-based energy management and the actual SOC controlled by NMPC has excellent following performance.

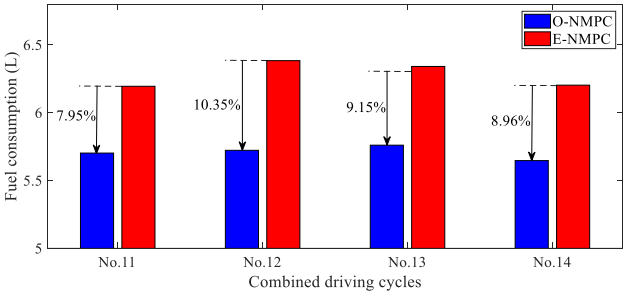

FIGURE 20. The fuel consumption of O-NMPC compared with E-NMPC.

D. SIMULATION RESULTS AND DISCUSSION

The combined driving cycles from No.11 to No.14 are applied to verify the effectiveness of the proposed method. To evaluate the NMPC-based energy management with optimization of engine operating zone (O-NMPC), the NMPC-based energy management with experience of engine operating zone (E-NMPC) and rule-based (RB) energy management are employed here. As we all know, the RB has been widely used in real-world conditions, and it is characterized by charge depletion mode (CD) and charge maintenance mode (CS) [28]. In the CD mode, the battery is the main power source, but in the CS mode, the engine is the main power source. As shown in Fig. 19, the SOC trajectories under four different combined driving cycles are obtained, and the initial SOCs of three control strategies are all designed as 0.8. It is noteworthy that the SOC trajectory of the RB shows a trend of rapid decline first and then flattens. However, the SOC trajectories of O-NMPC and E-NMPC decline gradually which is different from the RB.

As shown in Fig. 20, the fuel economy of the O-NMPC improved on average by 9.10% compared with the E-NMPC. As shown in Fig. 21, the main reason is that the engine operating points of O-NMPC are more concentrated in the

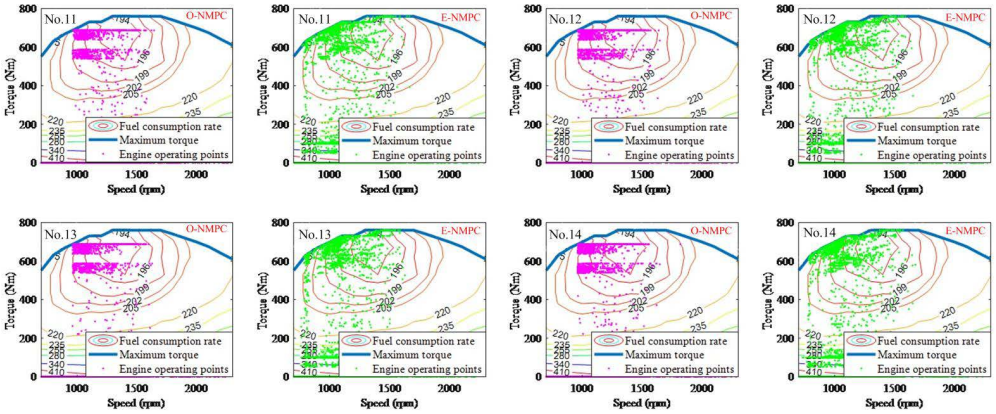

FIGURE 21. The engine operating points of the O-NMPC and the E-NMPC.

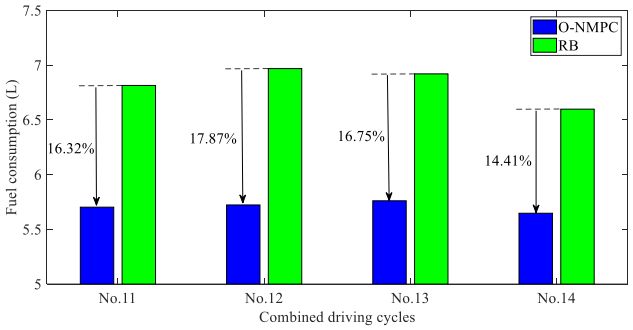

FIGURE 22. The fuel consumption of O-NMPC compared with RB.

high-efficiency zone than that of E-NMPC. Fig. 22 shows that the fuel economy of the O-NMPC is better than the RB, and it improved on average by 16.34% compared with the latter. The simulation results show that the proposed method is feasible, and the optimized engine operating zone has a significant effect on improving fuel economy.

VI. CONCLUSION

This paper proposes a robust design method to optimize the engine operating zone. The main conclusions are as follows.

1) The MCS reliable verification is deployed to verify the designed engine operating zone based on TRD, whose results demonstrate that the designed engine operating zone is reliable and robust, while there is still a 1% probability of failure.

2) For the proposed SOC reference trajectory based on the single-point preview, the experimental results demonstrate that the actual SOC has an excellent ability to follow the reference SOC. Most of the deviations between the actual SOC and the reference SOC locate in the scope of $[-2, 2]$.

3) The simulation results demonstrate that the proposed method can effectively improve the economy of PHEB. The fuel economy of the O-NMPC can be averagely improved by 9.10% compared with the E-NMPC, and be averagely improved by 16.34% compared with the RB.

The further research will concentrate on two aspects. (1) The proposed method should be further verified by real vehicles, because of the dynamic and stochastic characteristics of real traffic environment. (2) Since the design method of TRD is a general method, it can be further used in other strategies. For example, the SOC trajectory of the PHEB can be planned by the similar method to improve its fuel economy.

REFERENCES

[1] M. Mahmoodi-k, M. Montazeri, and V. Madanipour, "Simultaneous multi-objective optimization of a PHEV power management system and component sizing in real world traffic condition," *Energy*, vol. 233, Oct. 2021, Art. no. 121111.

[2] Y. Zhang, Y. Liu, Y. Huang, Z. Chen, G. Li, W. Hao, G. Cunningham, and J. Early, "An optimal control strategy design for plug-in hybrid electric vehicles based on internet of vehicles," *Energy*, vol. 228, Aug. 2021, Art. no. 120631.

[3] S. Li, C. Gu, P. Zhao, and S. Cheng, "Adaptive energy management for hybrid power system considering fuel economy and battery longevity," *Energy Convers. Manage.*, vol. 235, May 2021, Art. no. 114004.

[4] S. Zhou, Z. Chen, D. Huang, and T. Lin, "Model prediction and rule based energy management strategy for a plug-in hybrid electric vehicle with hybrid energy storage system," *IEEE Trans. Power Electron.*, vol. 36, no. 5, pp. 5926–5940, May 2021.

[5] Z. Chen, H. Zhang, R. Xiong, W. Shen, and B. Liu, "Energy management strategy of connected hybrid electric vehicles considering electricity and oil price fluctuations: A case study of ten typical cities in China," *J. Energy Storage*, vol. 36, Apr. 2021, Art. no. 102347.

[6] Z. Zhang, H. He, J. Guo, and R. Han, "Velocity prediction and profile optimization based real-time energy management strategy for plug-in hybrid electric buses," *Appl. Energy*, vol. 280, Dec. 2020, Art. no. 116001.

[7] S. Uebel, N. Murgovski, B. Baker, and J. Sjoberg, "A two-level MPC for energy management including velocity control of hybrid electric vehicles," *IEEE Trans. Veh. Technol.*, vol. 68, no. 6, pp. 5494–5505, Jun. 2019.

[8] B. Xu, J. Hou, J. Shi, H. Li, D. Rathod, Z. Wang, and Z. Filipi, "Learning time reduction using warm-start methods for a reinforcement learning-based supervisory control in hybrid electric vehicle applications," *IEEE Trans. Transport. Electrific.*, vol. 7, no. 2, pp. 626–635, Jun. 2021.

[9] X. Li and S. A. Evangelou, "Torque-leveling threshold-changing rule-based control for parallel hybrid electric vehicles," *IEEE Trans. Veh. Technol.*, vol. 68, no. 7, pp. 6509–6523, Jul. 2019.

[10] Q. Xu, X. Luo, X. Jiang, and M. Zhao, "Research on double fuzzy control strategy for parallel hybrid electric vehicle based on GA and DP optimisation," *IET Electr. Syst. Transp.*, vol. 8, no. 2, pp. 144–151, Jun. 2018.

[11] H. Zhou, Z. Xu, L. Liu, D. Liu, and L. Zhang, "A rule-based energy management strategy based on dynamic programming for hydraulic hybrid vehicles," *Math. Problems Eng.*, vol. 2018, pp. 1–10, Oct. 2018.

[12] J. Hu, J. Li, Z. Hu, L. Xu, and M. Ouyang, "Power distribution strategy of a dual-engine system for heavy-duty hybrid electric vehicles using dynamic programming," *Energy*, vol. 215, Jan. 2021, Art. no. 118851.
[13] A. Solouk, M. Shakiba-Herfeh, and M. Shahbakhti, "Analysis and control of a torque blended hybrid electric powertrain with a multi-mode LTC-Si engine," *SAE Int. J. Alternative Powertrains*, vol. 6, no. 1, pp. 54–67, Mar. 2017.
[14] X. Liu, D. Qin, and S. Wang, "Minimum energy management strategy of equivalent fuel consumption of hybrid electric vehicle based on improved global optimization equivalent factor," *Energies*, vol. 12, no. 11, p. 2076, May 2019.
[15] Z. Wang and X. Jiao, "Hierarchical model predictive control for hydraulic hybrid powertrain of a construction vehicle," *Appl. Sci.*, vol. 10, no. 3, p. 745, Jan. 2020.
[16] T. Liu, X. Tang, H. Wang, H. Yu, and X. Hu, "Adaptive hierarchical energy management design for a plug-in hybrid electric vehicle," *IEEE Trans. Veh. Technol.*, vol. 68, no. 12, pp. 11513–11522, Dec. 2019.
[17] W. Zhang, J. Wang, Y. Liu, G. Gao, S. Liang, and H. Ma, "Reinforcement learning-based intelligent energy management architecture for hybrid construction machinery," *Appl. Energy*, vol. 275, Oct. 2020, Art. no. 115401.
[18] M. Li, H. He, L. Feng, Y. Chen, and M. Yan, "Hierarchical predictive energy management of hybrid electric buses based on driver information," *J. Cleaner Prod.*, vol. 269, Oct. 2020, Art. no. 122374.
[19] R. M. Bagwe, A. Byerly, E. C. dos Santos, and Ben-Miled, "Adaptive rule-based energy management strategy for a parallel HEV," *Energies*, vol. 12, no. 23, p. 4472, Nov. 2019.
[20] J. Zhang, L. Chu, C. Guo, Z. Fu, and D. Zhao, "A novel energy management strategy design methodology of a PHEV based on data-driven approach and online signal analysis," *IEEE Access*, vol. 9, pp. 6018–6032, 2021.
[21] N. Guo, J. Shen, R. Xiao, W. Yan, and Z. Chen, "Energy management for plug-in hybrid electric vehicles considering optimal engine ON/OFF control and fast state-of-charge trajectory planning," *Energy*, vol. 163, pp. 457–474, Nov. 2018.
[22] W. Shabbir and S. A. Evangelou, "Threshold-changing control strategy for series hybrid electric vehicles," *Appl. Energy*, vol. 235, pp. 761–775, Feb. 2019.
[23] H. Guo, B. Liang, H. Guo, and K. Zhang, "A robust co-state predictive model for energy management of plug-in hybrid electric bus," *J. Cleaner Prod.*, vol. 250, Mar. 2020, Art. no. 119478.
[24] H. Guo, S. Lu, H. Hui, C. Bao, and J. Shangguan, "Receding horizon control-based energy management for plug-in hybrid electric buses using a predictive model of terminal SOC constraint in consideration of stochastic vehicle mass," *Energy*, vol. 176, pp. 292–308, Jun. 2019.
[25] J. Shangguan, H. Guo, and M. Yue, "Robust energy management of plug-in hybrid electric bus considering the uncertainties of driving cycles and vehicle mass," *Energy*, vol. 203, Jul. 2020, Art. no. 117836.
[26] Y. Wang, X. Wang, Y. Sun, and S. You, "Model predictive control strategy for energy optimization of series-parallel hybrid electric vehicle," *J. Cleaner Prod.*, vol. 199, pp. 348–358, Oct. 2018.
[27] J. Oncken and B. Chen, "Real-time model predictive powertrain control for a connected plug-in hybrid electric vehicle," *IEEE Trans. Veh. Technol.*, vol. 69, no. 8, pp. 8420–8432, Aug. 2020.
[28] Y. Liu, J. Gao, D. Qin, Y. Zhang, and Z. Lei, "Rule-corrected energy management strategy for hybrid electric vehicles based on operation-mode prediction," *J. Cleaner Prod.*, vol. 188, pp. 796–806, Jul. 2018.

YUJIE LIU received the B.E. degree in automobile engineering from Liaocheng University, Shandong, China, in 2019, where he is currently pursuing the Ph.D. degree with the School of Mechanical and Automotive Engineering.

His research interests include hybrid powertrain system and control, and intelligent vehicle dynamics and control.

QUN SUN received the Ph.D. degree in measurement techniques and instruments from Beihang University, in 2008.

He is currently a Professor at the School of Mechanical and Automotive Engineering, Liaocheng University, Shandong, China. His current research interests include robotics, and intelligent vehicle measurement and control.

QIANG HAN received the B.E. degree in automobile engineering from the Shandong University of Science and Technology, China, in 2011. He is currently pursuing the Ph.D. degree with the School of Mechanical and Automotive Engineering, Liaocheng University, Shandong, China. His research interests include hybrid powertrain system and control, and intelligent vehicle dynamics and control.

HAIGANG XU received the master's degree from the Shandong University of Science and Technology, Shandong, China, in 2019.

He is currently a Researcher at Shandong Shifeng (Group) Company Ltd., Shandong. His research interests include mechanical equipment design, and intelligent vehicle measurement and control.

WENXIAO HAN is currently pursuing the bachelor's degree with the School of Mechanical and Automotive Engineering, Liaocheng University, Shandong, China. His research interests include hybrid powertrain system and control, and intelligent vehicle dynamics and control.

HONG-QIANG GUO received the Ph.D. degree in mechanical engineering from the Beijing Institute of Technology, China, in 2014.

He is currently an Associate Professor at the School of Mechanical and Automotive Engineering, Liaocheng University, Shandong, China. His research interests include hybrid powertrain system and control, and intelligent vehicle dynamics and control.